

High-pressure synthesis of the BaIrO₃ perovskite: A Pauli paramagnetic metal with a Fermi liquid ground state

J.-G. Cheng,^{1,3,*} T. Ishii,² H. Kojitani,² K. Matsubayashi,¹ A. Matsuo,¹ X. Li,³ Y. Shirako,⁴ J.-S. Zhou,⁴ J. B. Goodenough,⁴ C. Q. Jin,³ M. Akaogi,² and Y. Uwatoko¹

¹*Institute for Solid State Physics, University of Tokyo, 5-1-5 Kashiwanoha, Kashiwa, Chiba 277-8581, Japan*

²*Department of Chemistry, Gakushuin University, 1-5-1 Mejiro, Toshima-ku, Tokyo 171-8588, Japan*

³*Beijing National Laboratory for Condensed Matter Physics and Institute of Physics, Chinese Academy of Sciences, Beijing 100190, China*

⁴*Materials Science and Engineering Program/Mechanical Engineering, University of Texas at Austin, Texas 78712, USA*

(Received 1 September 2013; revised manuscript received 19 October 2013; published 12 November 2013)

BaIrO₃ adopts the 9R polytype structure if it is synthesized at ambient pressure. High-pressure and high-temperature treatments up to 10 GPa have led to other 5H and 6H polytype phases, which are quenchable to the ambient condition. However, the single-phase 3C perovskite, the end member of polytypes, has not been obtained so far. Here we report the high-pressure synthesis of BaIrO₃ perovskite under 25 GPa and 1150 °C. Rietveld refinement on the powder x-ray diffraction pattern revealed that this new compound crystallizes in a tetragonal *I4/mcm* structure rather than the expected cubic *Pm-3m* structure. The new perovskite is a Pauli paramagnetic metal with a Fermi liquid ground state, i.e., $\rho \propto T^2$ below 6 K. The availability of BaIrO₃ perovskite also allows completion of the structure-physical property evolution in the AIrO₃ perovskites (*A* = Ca, Sr, Ba). The Fermi energy located in bands originated from Ir: *5d* and O: *2p* electrons are found to be very sensitive to the change of crystal structure.

DOI: [10.1103/PhysRevB.88.205114](https://doi.org/10.1103/PhysRevB.88.205114)

PACS number(s): 71.55.Ak, 71.10.Ay, 71.70.Ej, 72.15.-v

I. INTRODUCTION

Recently, iridium oxides with perovskite-related structures have attracted much attention owing to the emergence of novel electronic states associated with a large spin-orbit coupling (SOC) on the heavy Ir atom. One such state is the effective total angular momentum $J_{\text{eff}} = 1/2$ state.^{1,2} In order to explain the insulating ground state of single-layer Sr₂IrO₄, Kim *et al.*¹ proposed that the *t*_{2g} band of low-spin Ir⁴⁺ (*5d*⁵) in an octahedral site splits into a lower energy $J_{\text{eff}} = 3/2$ quartet band and a high-energy $J_{\text{eff}} = 1/2$ doublet band in the strong SOC limit. As a result, a moderate on-site Coulomb repulsion *U* can open a Mott gap within the narrow, half-filled $J_{\text{eff}} = 1/2$ band, leading to a SOC-driven Mott insulating state. Although the electronic correlation energy, *U* ~ 0.5 eV, is relatively small in these *5d* oxides, SOC amplifies the effect of *U* through narrowing the bandwidth (*W*) of the conduction $J_{\text{eff}} = 1/2$ band. As a consequence, the magnetic insulating ground state prevails in the postperovskite CaIrO₃ and the nine-layer (9R) BaIrO₃ (Refs. 3 and 4).

Although a bandwidth-controlled insulator-to-metal transition has been reported in the Ruddlesden-Popper series Sr_{*n*+1}Ir_{*n*}O_{3*n*+1} with increasing number *n* of perovskite layers, which closes up the gap due to correlations in the $J_{\text{eff}} = 1/2$ band,⁵ the three-dimensional perovskite SrIrO₃ (*n* = ∞) was found to be a strange metal, as manifested by a broad upturn of resistivity at low temperatures.⁶ Such an unusual behavior can be rationalized in light of the recent theoretical analysis by Carter *et al.*^{7,8} Their first-principles calculations on the orthorhombic SrIrO₃ perovskite revealed that (1) SOC renormalizes strongly the band structure and retains the $J_{\text{eff}} = 1/2$ band near the Fermi level, and (2) the reflection symmetry at the $z = \frac{1}{4}$ and $\frac{3}{4}$ planes of the orthorhombic lattice results in a robust line node within the $J_{\text{eff}} = 1/2$ band near the Fermi level, leading to a semimetal state with a small

density of states at *E*_{*F*}. Although the six-layer (6H) SrIrO₃, the ambient-pressure polymorph of the perovskite phase,⁹ is metallic down to the lowest temperature, a non-Fermi liquid (nFL) ground state has been reported due to the proximity to a magnetic quantum critical point (QCP).¹⁰ However, a metallic phase, especially having a Fermi liquid ground state, derived from a half-filled $J_{\text{eff}} = 1/2$ band has not been seen in the stoichiometric Ir⁴⁺ oxides to date.

The BaIrO₃ perovskite would be an ideal candidate to be a Pauli paramagnetic metal. Because of its tolerance factor $t \equiv (\text{Ba}-\text{O})/\sqrt{2}(\text{Ir}-\text{O}) = 1.05 > 1$, however, BaIrO₃ adopts at ambient pressure a monoclinically distorted nine-layer (9R) structure consisting of Ir₃O₁₂ trimers of face-sharing octahedra linked via vertex sharing to form quasi-one-dimensional (1D) columns along the *c* axis. Equivalently, the crystal structure can be described as a stacking of layers of corner-sharing (C) and face-sharing (F) IrO_{6/2} octahedra in the sequence CFFCFFCFF along the *c* axis. As mentioned above, this compound is a weak ferromagnetic insulator.⁴ By treating the 9R phase at 1000 °C under various pressures up to 10 GPa, we have obtained three more polytypes, i.e., 5H, 6H, and 3C.¹¹ Among them, the former two can be stabilized as single-phase compounds. Although they are found to be metallic in general, the resistivity of the 5H phase exhibits a sudden drop at about 3.4 K followed by a semiconductor behavior on further cooling.¹² Similar to the aforementioned 6H SrIrO₃, the 6H BaIrO₃ also displays nFL behavior, i.e., $\rho \propto T^{5/3}$, in the vicinity of a QCP.¹² On the other hand, the perovskite 3C phase was only identified as a minor phase (~5%) that coexists with the 6H phase in a high-pressure synthesis under 10 GPa, the highest pressure in our previous study.¹¹ Much higher pressures are required in order to stabilize a phase-pure BaIrO₃ perovskite. Following this lead, we have been searching for the single-phase BaIrO₃ perovskite in an extended pressure range by using state-of-the-art multianvil high-pressure techniques.

In this paper, we report for the first time the synthesis of single-phase BaIrO₃ perovskite under 25 GPa and 1150 °C followed by a detailed characterizations of its crystal structure and physical properties. Surprisingly, the obtained BaIrO₃ perovskite adopts a tetragonal *I4/mcm* structure rather than the expected cubic *Pm-3m* structure. In addition, it was found to be a Pauli paramagnetic metal exhibiting a Fermi liquid behavior at low temperatures. Thus, the BaIrO₃ perovskite represents the only case of a Fermi liquid metal among the known stoichiometric Ir⁴⁺ oxides. Moreover, the availability of BaIrO₃ perovskite enables us to finally complete the structure-physical property evolutions in the BaIrO₃ polytypes and the AIrO₃ perovskites (*A* = Ca, Sr, Ba). It has been shown that physical properties are extremely sensitive to the crystal structure.

II. EXPERIMENTAL

High-pressure and high-temperature (HPHT) syntheses in the present study were carried out with a Kawai-type multianvil apparatus at Gakushuin University.¹³ Tungsten carbide (WC) anvils of 5-mm truncated edge length (TEL) and a semisintered MgO octahedron of 10-mm edge length (EL) were used for HPHT syntheses up to 18 GPa; WC anvils of 2.5-mm TEL and an MgO octahedron of 5-mm EL were used for syntheses up to 25 GPa. Temperature was monitored by an R-type (Pt/Pt-13%Rh) thermocouple with the hot junction positioned in the center of the Pt furnace.

Phase purity of the recovered high-pressure products was examined by powder x-ray diffraction (XRD) at room temperature with a Rigaku RINT 2500 diffractometer (Cr K_α, 45 kV, 250 mA). The XRD pattern recorded in the 2θ range 20–140° with a step size 0.02° and a dwell time 12 s was analyzed with the Rietveld method by using the software RIETAN-FP.¹⁴ The split pseudo-Voigt function of Toraya¹⁵ was used as a profile function. The surface roughness with Sidey's model¹⁶ was also refined in the Rietveld analysis. Atomic displacement parameters of oxygen were fixed to 0.8 Å². Magnetic properties were measured with a commercial superconducting quantum interference device (SQUID) magnetometer (Quantum Design). Measurements of electrical resistivity and specific heat were performed in a Physical Property Measurement System (Quantum Design).

III. RESULTS AND DISCUSSION

In our previous study,¹¹ we have shown that the ambient 9R phase is stable up to 3 GPa; it transforms to a new 5H phase at about 4 GPa and then to the 6H phase at 5 GPa. Our present study further shows that the 6H phase remains stable up to 18 GPa at 1000 °C. We finally obtained a single-phase BaIrO₃ perovskite at 25 GPa and 1150 °C. Its powder XRD pattern shown in Fig. 1 displays a clear peak splitting, especially at high angles (inset of Fig. 1), which indicates that the BaIrO₃ perovskite adopts a lower symmetry than the expected cubic structure with the space group *Pm-3m*. Indeed, the XRD pattern in Fig. 1 can be refined excellently in the tetragonal *I4/mcm* (No. 140) space group with the Ba atom at 4*b* (0, 1/2, 1/4), the Ir atom at 4*c* (0, 0, 0), and O atoms at 4*a* (0, 0, 1/4) and 8*h* (*x*, *x* + 1/2, 0) sites. In addition, a

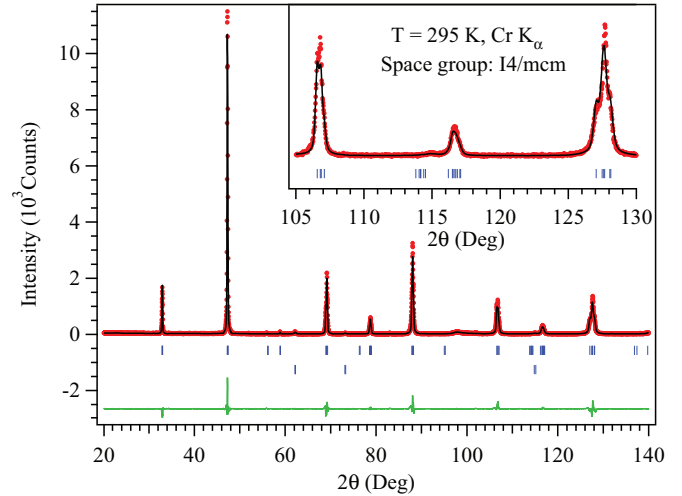


FIG. 1. (Color online) Rietveld refinement of the powder XRD pattern of BaIrO₃ perovskite synthesized at 25 GPa and 1150 °C. Inset shows the profile at high angles between 105° and 130°, illustrating the peak splitting due to a tetragonal symmetry.

trace amount of Ir impurity, ~1.0 wt.%, is evidenced from the XRD refinement. The final atomic parameters and the main interatomic distances and angles after Rietveld refinements are given in Tables I and II, respectively.

The small tetragonal distortion of the 3C BaIrO₃ phase is unexpected; we should have a cubic phase as found for BaRuO₃ formed under high pressure.¹⁷ Based on the measured unit-cell parameters $a = b = 5.7044(1)$ Å and $c = 8.0926(2)$ Å, the tetragonal $\sqrt{2} a/c = 0.997$ ratio is too small to have been resolved in our previous sample with a minor 3C phase.¹¹ Such a distortion to tetragonal symmetry by cooperative rotations of the IrO_{6/2} octahedra about the *c* axis is typical of an A²⁺B⁴⁺O₃ perovskite with a tolerance factor $t \equiv (A-O)/[\sqrt{2}(B-O)]$ a little smaller than unity. However, stabilization of BaIrO₃ in the 9R polytype at ambient pressure is consistent with $t > 1$ obtained from tabulated equilibrium ionic radii. The larger compressibility of the Ba–O bond makes it possible to stabilize the 3C phase of BaIrO₃ under 25 GPa pressure, but compression of the Ba–O bond by cubic symmetry should not reduce the tolerance factor below $t = 1$. Retention of the cubic symmetry of the IrO_{6/2} octahedra shows that the threefold degeneracy of the 5*d* π* bands is not a factor. In fact, the tolerance factor calculated from the measured ⟨Ba–O⟩ and ⟨Ir–O⟩ bond lengths in Table II gives a $t = 0.998$

TABLE I. Atomic coordinates and isotropic thermal factors B_{iso} [Å²] for BaIrO₃ perovskite from powder XRD data at 295 K;^a space group *I4/mcm* (No. 140), $a = b = 5.7044(1)$ Å, $c = 8.0916(2)$ Å, $V = 263.30(1)$ Å³, $Z = 4$.

Atom	Site	<i>x</i>	<i>y</i>	<i>z</i>	B_{iso}
Ba	4 <i>b</i>	0	0.5	0.25	0.72(4)
Ir	4 <i>c</i>	0	0	0	0.49(1)
O1	4 <i>a</i>	0	0	0.25	0.8
O2	8 <i>h</i>	0.2313(3)	0.7313(3)	0	0.8

^aDiscrepancy factors: $R_p = 10.65\%$, $R_{\text{WP}} = 15.9\%$, $R_{\text{exp}} = 10.57\%$, $R_{\text{Bragg}} = 3.38\%$.

TABLE II. Main interatomic distances (Å) and angles (°) of BaIrO₃ perovskite from powder XRD data at 295 K.

Bond length (Å)		Bond angle (°)	
Ba–O1 (×4)	2.8522(1)	O1–Ir–O2	90.0(7)
Ba–O2 (×4)	2.969(2)	O1–Ir–O2	90.0(7)
Ba–O2 (×4)	2.748(2)	O2–Ir–O2	90.0(1)
⟨Ba–O⟩	2.857		
Ir–O1 (×2)	2.023 (1)	Ir–O1–Ir	180.0
Ir–O2 (×4)	2.023(2)	Ir–O2–Ir	171.1(1)
⟨Ir–O⟩	2.023	⟨Ir–O–Ir⟩	174.1

consistent with the tetragonal structure observed. Therefore, we conclude that at 25 GPa there has been a first-order transition of the Ba–O equilibrium bond length to give a $t < 1$, which indicates that the $5d\pi^*$ bands of the IrO_{6/2} array may also have transitioned for $J_{\text{eff}} = 1/2$ and $3/2$ bands as a result of a reduction of the orbital angular momentum where the bandwidth is broadened. The high-pressure equilibrium (Ba–O) bond length is retained as a metastable bond length on removal of the pressure, and the Ir–O bonds are not under a tensile stress.

Consistent with the nearly cubic structure of the BaIrO₃ perovskite, our physical properties measurements demonstrate that the bandwidth of the IrO_{6/2} array is indeed broad enough to ensure a Fermi liquid ground state. As shown in Fig. 2(a), the 3C BaIrO₃ remains metallic down to at least 1.8 K, the lowest temperature in the present study. The resistivity $\rho(T)$ displays a saturation behavior at high temperatures; it follows the Fermi liquid behavior, *vi z.* $\rho \propto T^2$, at low temperatures. As shown in

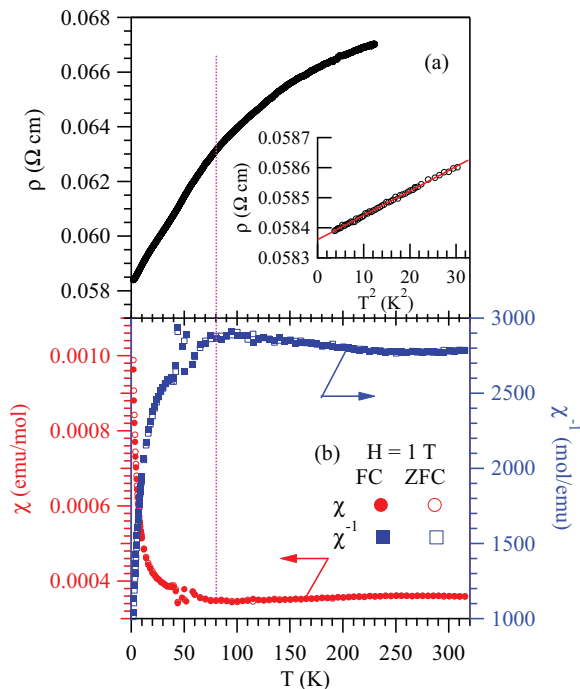


FIG. 2. (Color online) Temperature dependence of (a) resistivity $\rho(T)$ and (b) magnetic susceptibility $\chi(T)$ of the BaIrO₃ perovskite. Inset of (a) displays the $\rho(T)$ data below 6 K in the form of ρ vs T^2 as well as a linear fitting.

the inset of Fig. 2(a), a linear fitting to $\rho(T) = \rho_0 + AT^2$ below 6 K yields $\rho_0 = 0.0584(1) \Omega \text{ cm}$ and $A = 8.1(1) \mu\Omega \text{ cm K}^{-2}$, respectively. The relatively high resistivity and small residual resistivity ratio $\rho(300 \text{ K})/\rho_0$ observed in Fig. 2(a) should arise from the grain boundary effect of the polycrystalline sample as well as any residual strain after recovery from treatment under high pressure.

Figure 2(b) shows the temperature dependence of magnetic susceptibility $\chi(T)$ and its inverse $\chi^{-1}(T)$ measured upon heating from 1.8 to 300 K under $H = 1 \text{ T}$ after zero-field cooling (ZFC) and field cooling (FC). The ZFC and FC $\chi(T)$ curves are completely overlapped with each other in the whole temperature range and exhibit a nearly temperature-independent Pauli paramagnetism. The low-temperature upturn should be ascribed to defects or impurity spins. It is interesting to note that the $\chi(T)$ curves display a shallow minimum around 85 K, where $\rho(T)$ exhibits a slope change, as indicated by the dotted line in Fig. 2(a). A similar dip in $\chi(T)$ and a corresponding kinklike anomaly in $\rho(T)$ at $T^* \approx 170 \text{ K}$ have also been reported in the SrIrO₃ perovskite.⁶ Whether this feature in these perovskite iridates arises from a subtle change of electronic structure deserves further study.

Figure 3 shows the specific heat $C(T)$ of 3C BaIrO₃ measured in the temperature range 1.8–200 K under $H = 0$ and 5 T. In line with the paramagnetic and metallic behavior shown above, no anomaly can be discerned in the measured temperature range. The effect of a magnetic field on $C(T)$ is also negligible. In order to separate the contributions from electrons and lattice, we have replotted in the inset of Fig. 3 the $C(T)$ data between 1.8–12 K in the form of C/T vs T^2 and fitted it with the formula $C/T = \gamma + \beta T^2 + \delta T^4$, where the first term describes the electronic contribution and the second and third terms represent the lattice contribution. As shown by the solid line, the best fitting gives $\gamma = 6.84(6) \text{ mJ/mol K}^2$, $\beta = 0.257(2) \text{ mJ/mol K}^4$, and $\delta = 0.15(1) \mu\text{J/mol K}^6$, respectively. The Debye temperature $\Theta_D = 335 \text{ K}$ was calculated according to $\Theta_D = (12\pi^4 n R / 5\beta)^{1/3}$, where $n = 5$ is the number of atoms in the chemical formula and R is the ideal gas constant.

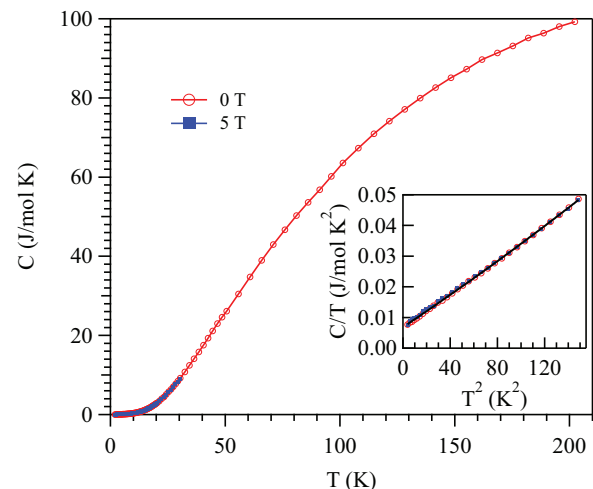


FIG. 3. (Color online) Specific heat $C(T)$ of BaIrO₃ perovskite measured under $H = 0$ and 5 T. Inset shows the low-temperature region in the plot of C/T vs T^2 .

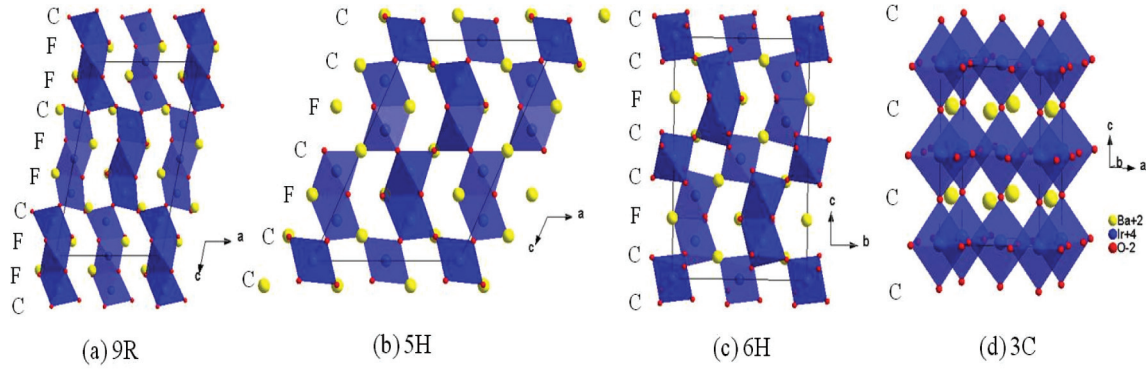


FIG. 4. (Color online) Evolution of the crystal structures of BaIrO_3 polytypes: (a) 9R, (b) 5H, (c) 6H, and (d) 3C. The letters on the side of crystal structure denote the stacking sequence of IrO_6 octahedron, C for corner sharing and F for face-sharing.

Based on the above characterizations, we have established the following: (1) the single-phase BaIrO_3 perovskite can be obtained under 25 GPa and 1150 °C; (2) it adopts a tetragonal $I4/mcm$ space group; and (3) it is a Pauli paramagnetic metal with a Fermi liquid behavior. Such a ground state distinguishes it from existing stoichiometric Ir^{4+} oxides with perovskite-related structures. As mentioned above, strong SOC renormalizes the broad t_{2g} band and leaves a narrow half-filled $J_{\text{eff}} = 1/2$ conduction band near the Fermi level. When the $J_{\text{eff}} = 1/2$ bandwidth (W) is further reduced by a lower structural dimensionality, a relatively small on-site U can open a Mott gap and lead to an insulating ground state that is commonly accompanied by a peculiar magnetic ordering. Such a situation is found to be prevailing in the existing iridates, such as the nine-layer BaIrO_3 with quasi-1D structure,⁴ the K_2NiF_4 -type Sr_2IrO_4 (Ref. 17), and the postperovskite CaIrO_3 (Refs. 3 and 18) with quasi-two-dimensional structures. Even in the three-dimensional perovskites CaIrO_3 and SrIrO_3 , the orthorhombic distortions resulting from the rotation and tilting of the corner-sharing $\text{IrO}_{6/2}$ octahedra also reduced W to the boundary of metal-to-insulator transition, as evidenced by the resistivity upturn at low temperatures.^{6,18,19} Although a metallic conduction has been observed in the 6H SrIrO_3 (Ref. 10) and 6H BaIrO_3 (Refs. 12 and 20), their resistivity data follow the nFL behavior, i.e., $\rho \propto T^n$, with $n = 3/2$ and $5/3$, respectively, due to the proximity to a magnetic QCP. In this sense, therefore, the perovskite BaIrO_3 stands out of the existing iridates as a Pauli paramagnetic Fermi liquid metal.

The availability of BaIrO_3 perovskite enables us to complete the crystal structure-physical property evolution in two series: the BaIrO_3 polytypes and the AIrO_3 perovskites ($A = \text{Ca}, \text{Sr}, \text{Ba}$). In both cases, the physical properties are very sensitive to the structural changes.

A. BaIrO_3 polytypes

The polytype structures of ABO_3 oxides and the phase transformations under high pressure were intensively studied in the 1960s and the 1970s (Ref. 21); the classical sequence of $2\text{H} \rightarrow 9\text{R} \rightarrow 4\text{H} \rightarrow 6\text{H} \rightarrow 3\text{C}$ as a function of increasing pressure has been well-established. However, successive phase transitions involving more than three polytypes for a given ABO_3 oxide were hardly seen due to the limited pressure capacity available in the early days. Recent progress in

high-pressure capacity makes this task possible and, more importantly, enables one to elucidate the intimate relationship between the crystal structure and physical properties in these polytypes with subtle structure variations. One of the most prominent examples in this regard comes from the recent synthesis of cubic BaRuO_3 perovskite under 18 GPa with state-of-the-art multi-anvil high-pressure techniques.²² The availability of cubic BaRuO_3 not only completed for the first time the whole polytype sequence from 9R to 3C that has been known for over 40 years but also provided an important clue for understanding the unusual ferromagnetism in perovskite ruthenates.

Motivated by the work on BaRuO_3 , we initiated the study on BaIrO_3 and found a new 5H polytype in the high-pressure sequence, i.e., $9\text{R} \rightarrow 5\text{H} \rightarrow 6\text{H} \rightarrow 3\text{C}$. Such a novel polytype sequence that is unlike the classical $9\text{R} \rightarrow 4\text{H} \rightarrow 6\text{H} \rightarrow 3\text{C}$, as displayed by BaRuO_3 , has been ascribed to the compromise between the strong Ir–Ir bonding and the Coulombic repulsion across the shared faces between octahedra. In our previous study,¹¹ the end-member 3C phase was described as a simple cubic $Pm-3m$ perovskite owing to the lower concentration of the perovskite phase in a sample with the predominant 6H phase. The evolution of crystal structures for these polytypes is illustrated in Fig. 4. As can be seen, the major change of these polytypes can be described by the stacking sequence of IrO_6 octahedra that evolves from $9\text{R}(\text{CFFCFFCFF}) \rightarrow 5\text{H}(\text{CFCCF}) \rightarrow 6\text{H}(\text{CCFCCF}) \rightarrow 3\text{C}(\text{CCC})$, where C and F stands for corner- and face-sharing, respectively. The specific structural features for each polytype have been discussed in detail in our previous paper.¹¹ The present observation of tetragonal symmetry of the 3C phase does not affect the discussion and major conclusions in our previous study about their crystal structures.

As illustrated in Fig. 5, with increasing C:F ratio in the sequence $9\text{R}(1:2) \rightarrow 5\text{H}(3:2) \rightarrow 6\text{H}(2:1) \rightarrow 3\text{C}(\infty)$, the ground states of BaIrO_3 evolve from a ferromagnetic insulator with $T_c = 180$ K in the 9R phase to a ferromagnetic metal with $T_c = 50$ K in the 5H phase, then to an exchange-enhanced paramagnetic metal with nFL behavior near a QCP in the 6H phase, and finally to a Fermi liquid metal in the 3C phase. Such a structure-physical property evolution has been ascribed to a progressive bandwidth broadening in the sense that the corner-shared arrangement of IrO_6 octahedra can facilitate the Ir overlap integral mediated via $\text{O}-2p$ orbitals. Since

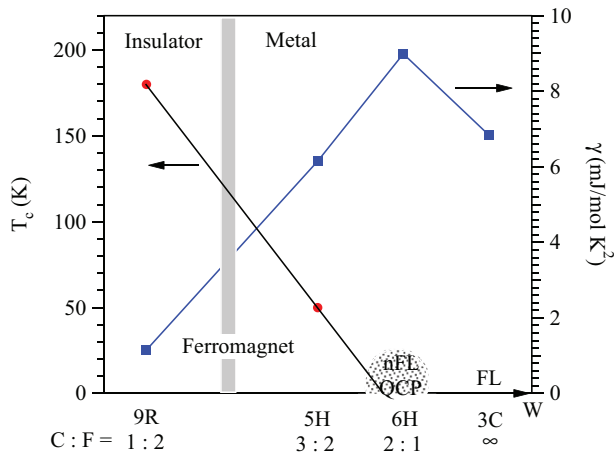


FIG. 5. (Color online) A schematic phase diagram of the BaIrO₃ polytypes showing the evolution of magnetic transition temperature T_c (left) and the electronic specific-heat coefficient γ (right) as a function of the C:F ratio.

the electronic specific-heat coefficient γ is proportional to the density of states at the Fermi energy, the gradual enhancement of γ from 9R to 6H phase shown in Fig. 5 is in agreement with the bandwidth argument. Both the 6H and 3C phase are metallic. Since the 6H phase is close to a QCP, the γ is much enhanced due to critical fluctuations relative to that in the 3C phase with an even broader bandwidth.

BaIrO₃ becomes the second ABO₃ oxide system that displays successive phase transitions involving more than three polytypes. More interestingly, both BaIrO₃ and BaRuO₃ reveal a progressive evolution of magnetic ground state from nonmagnetic to ferromagnetic accompanying the structure change. We make a side-by-side comparison of their magnetic susceptibility $\chi(T)$ in Fig. 6. For clarity, the $\chi(T)$ data in Figs. 6(a), 6(c) are shown in a semi-log scale. For BaRuO₃, the 9R phase displays a nonmagnetic ground state with a shallow minimum in $\chi(T)$ or a hump in the $\chi^{-1}(T)$ plot. This feature diminishes gradually and the Curie-Weiss (CW) behavior is

restored with increasing C:F ratio. Finally, in the 3C phase a long-range ferromagnetic ordering takes place below $T_c = 60$ K (Ref. 22); a CW fitting to the paramagnetic susceptibility yields an effective moment $\mu_{\text{eff}} = 2.6 \mu_B/\text{Ru}^{4+}$ that is close to the spin-only value of $2.83 \mu_B/\text{Ru}^{4+}$. The unusual $\chi(T)$ curve of the 9R phase as well as its evolution in the BaRuO₃ family has been explained in terms of a competition between SOC and the spin-spin exchange interaction,²² i.e., SOC can alter the ferromagnetic spin-spin exchange interactions. However, the corner-sharing octahedra in the 3C phase enhance the Ru-O-Ru spin-spin exchange interaction. The $\chi^{-1}(T)$ curve in Fig. 6(b) has been regarded as characteristic for SOC in the ruthenates and has been used further to explain the disappearance of ferromagnetism in the perovskite CaRuO₃.

In contrast to the BaRuO₃ polytypes, two members of the BaIrO₃ polytypes are magnetic: the ambient 9R phase exhibits a weak ferromagnetic transition with a $T_c = 180$ K, and the 5H phase displays a weak ferromagnetic transition at $T_c = 50$ K. Previous studies have shown that the magnetic transition in the 9R phase is accompanied by a simultaneous metal-insulator transition owing to a charge density wave formation.⁴ In contrast to the 3C BaRuO₃, the $\chi^{-1}(T)$ in the paramagnetic region of 9R BaIrO₃ does not follow the conventional CW behavior. Although $\chi^{-1}(T)$ above T_c can be described satisfactorily with the modified CW law, viz. $\chi = \chi_0 + C/(T - \theta)$, by adding a large constant term $\chi_0 = 2.08(1) \times 10^{-4}$ emu/mol, the obtained $\mu_{\text{eff}} = 0.186(6) \mu_B/\text{Ir}^{4+}$ is much smaller than the expected value for low-spin Ir⁴⁺ ($S = \frac{1}{2}$).¹² Such a reduced μ_{eff} is commonly seen in iridates. In the 5H BaIrO₃, the metallic resistivity exhibits an anomaly at T_c seen in most metallic ferromagnets such as 3C BaRuO₃ (Ref. 22). As pointed out earlier, such a metallic and ferromagnetic ground state is rarely seen among the known iridates and is associated with a delicate structural arrangement having mixed corner- and face-sharing octahedra. This observation demonstrates once again the merit of high-pressure synthesis in fine tuning the electronic ground states via subtle structure variations among these polytypes. With further increase of the C:F ratio in the 6H and 3C phases, their bandwidths are broad enough to suppress any long-range magnetic ordering. However, as shown in Fig. 6(d), an exchange-enhanced Pauli paramagnetism is clearly visible in the 6H phase but not in the 3C phase. The unusual $\chi^{-1}(T)$ curve for the 3C BaIrO₃ looks similar to that of the 9R BaRuO₃ phase; this similarity may signal suppression in the 3C BaIrO₃ phase of the strong SOC that creates $J_{\text{eff}} = 1/2$ and $3/2$ bands.

B. AIrO₃ perovskites (A = Ca, Sr, Ba)

Recent band-structure calculations^{7,8} on the orthorhombic SrIrO₃ perovskite revealed that (1) SOC narrows down the conduction band to be composed of mainly $J_{\text{eff}} = 1/2$ bands and (2) there exists near the Fermi level a robust Dirac nodal line protected by the reflection symmetry of the orthorhombic lattice. Thus, the combined effects of SOC and orthorhombic distortion in SrIrO₃ render a semimetal state characterized by a small density of states near the Fermi energy. Such a ground state is consistent with the experimental observations of the following⁶: (1) an upturn of resistivity below ~ 50 K, and (2) an electronic specific-heat coefficient as small as $\gamma = 2.5$ mJ/mol K². However, the aforementioned calculations

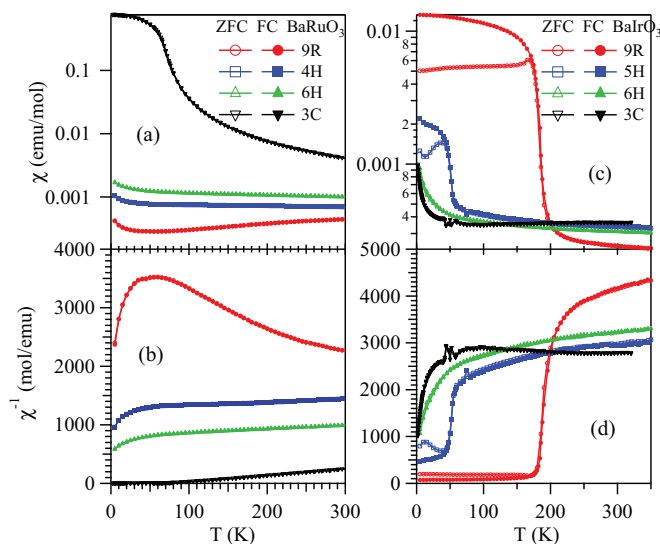


FIG. 6. (Color online) Magnetic susceptibility of (a), (b) BaRuO₃ and (c), (d) BaIrO₃ polytypes.

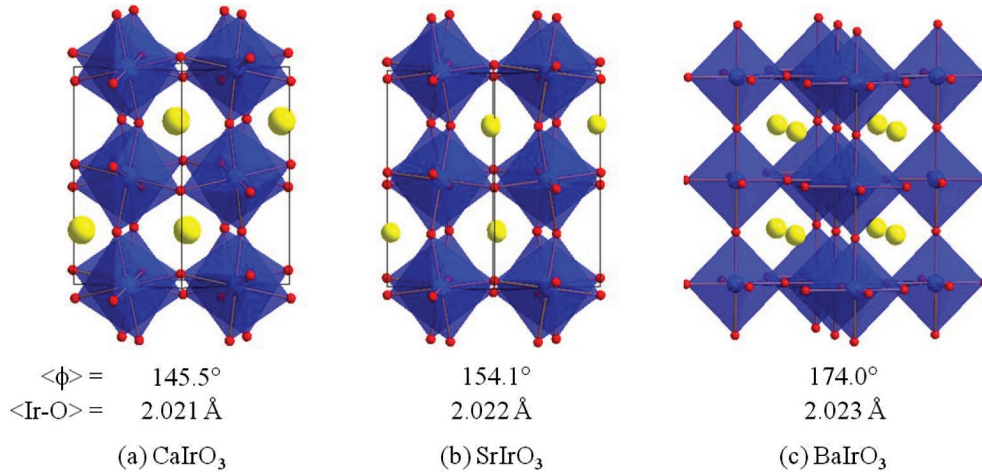


FIG. 7. (Color online) Crystal structures of the AIrO_3 perovskites ($A = \text{Ca}, \text{Sr}, \text{Ba}$), illustrating the gradual reduction of octahedral rotation with increasing the A -cation size. The values of average Ir–O–Ir bond angle $\langle\phi\rangle$ and average Ir–O bond length $\langle\text{Ir-O}\rangle$ for each phase are listed under the structure.

do not provide an evolution of the band structure as a function of orthorhombic distortion or even accompanying a change of lattice symmetry. The availability of BaIrO_3 perovskite offers an excellent opportunity to evaluate the ground state of perovskite iridates to a greater extent. Here, we would like to point out the evolution of physical properties as a function of structural distortion from an experimental point of view, which we hope will stimulate in-depth theoretical calculations.

Figure 7 shows the crystal structures of the $3\text{C}\text{A}\text{IrO}_3$ perovskites ($A = \text{Ca}, \text{Sr}, \text{Ba}$) consisting of a three-dimensional network of corner-sharing $\text{IrO}_{6/2}$ octahedra. The detailed structure information for perovskite CaIrO_3 has been given elsewhere.¹⁸ Both CaIrO_3 and SrIrO_3 adopt the orthorhombic $Pbnm$ structure arising from a cooperative rotation of IrO_6 octahedra about the cubic $[110]$ axis, which results in the deviation from the ideal 180° of Ir–O–Ir angles. With increasing

A -cation size, the orthorhombic distortion decreases and the average Ir–O–Ir bond angle $\langle\phi\rangle$ increases from 145.5° for CaIrO_3 to 154.1° for SrIrO_3 . A slight tetragonal distortion of BaIrO_3 perovskite results in a nearly straight Ir–O–Ir bond with an average $\langle\phi\rangle = 174^\circ$. On the other hand, the average Ir–O bond lengths $d = 2.021\text{--}2.023 \text{ \AA}$ for these three samples keep nearly constant and are consistent with the ionic radii sum for Ir^{4+} (0.625 \AA) and O^{2-} (1.40 \AA). This observation indicates that the bond-length mismatch is relieved mainly via the octahedral rotation in the CaIrO_3 and SrIrO_3 perovskites. But it remains a puzzle why a compressed Ba–O bond does not in turn stretch the Ir–O bond length in BaIrO_3 unless the equilibrium Ba–O bond length is changed to make $t < 1$. These structural features can thus increase the bandwidth, via a first-order approximation²³ $W \propto \cos(180^\circ - \phi)/d^{3.5}$, in these isostructural compounds. In agreement with this expectation, the resistivity data shown in Fig. 8 indeed reveal a progressive change from the conductor CaIrO_3 through the semimetal SrIrO_3 to the Fermi liquid metal BaIrO_3 . The nondivergent T dependence in the resistivity of the CaIrO_3 perovskite indicates that the band gap does not open completely within the $J_{\text{eff}} = 1/2$ band; the Fermi level may be located inside a pseudogap of lower Hubbard band and upper Hubbard band of $J_{\text{eff}} = 1/2$ states. With increasing bandwidth of the $J_{\text{eff}} = 1/2$ band from Ca to Sr to Ba, the density of states at the Fermi level would be enhanced accordingly, consistent with the increase of electronic specific-heat coefficient γ from 2.5 mJ/mol K^2 for SrIrO_3 to 6.8 mJ/mol K^2 for BaIrO_3 . On the other hand, a further bandwidth reduction in the two-dimensional postperovskite CaIrO_3 finally leads to a $J_{\text{eff}} = 1/2$ Mott insulating state.²⁴

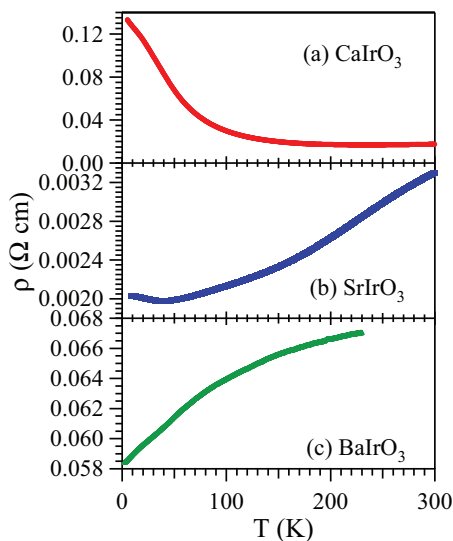


FIG. 8. (Color online) Resistivity of the AIrO_3 perovskites ($A = \text{Ca}, \text{Sr}, \text{Ba}$), illustrating the gradual change of electronic state from a conductor through a semimetal and to a metal with increasing A -cation size.

IV. CONCLUSIONS

In conclusion, the BaIrO_3 perovskite was successfully synthesized under 25 GPa and 1150°C with a multianvil high-pressure apparatus. Rather than the expected cubic $Pm\bar{3}m$ structure, it was found to adopt a tetragonal $I4/mcm$ structure. Measurements of physical properties confirmed that it is a

Pauli paramagnetic metal with Fermi liquid behavior at low temperatures. Such a ground state distinguishes it from the known stoichiometric Ir⁴⁺ oxides. The availability of BaIrO₃ perovskite enables us to see a complete evolution of physical properties as a function of subtle structure variations in two closely related structural systems. With increasing fraction of cubic stacking in the BaIrO₃ polytypes, the bandwidth of Ir-O-Ir array increases so that the phase diagram covers a rich evolution of ground states, including a weak ferromagnetic insulator, a weak ferromagnetic metal, an exchange-enhanced paramagnetic metal close to a QCP, and a Fermi liquid paramagnetic metal. On the other hand, straightening of Ir-O-Ir bond angle with a nearly constant Ir-O bond length across the AIrO₃ perovskites ($A = \text{Ca, Sr, Ba}$) broadens up the bandwidth of the $J_{\text{eff}} = 1/2$ band so as to induce a crossover of resistivity from conductor through semimetal to Fermi liquid metal. However, two questions remain with respect to the 3C

BaIrO₃ phase: (1) What causes the apparent change from a tolerance factor $t > 1$ at ambient pressure to a $t < 1$ after treatment at 25 GPa? (2) Does the strong SOC separation into $J_{\text{eff}} = 1/2$ and $J_{\text{eff}} = 3/2$ bands still apply in the Pauli paramagnetic metallic 3C phase?

ACKNOWLEDGMENTS

This work was partially supported by Grant-in-Aid for Scientific Research in Japan (Grants No. 12F02023, No. 23340101, No. 24740220, No. 252460135, and No. 25287145), Chinese Academy of Sciences, NSF, and MOST of China (Grants No. Y2K5016X51, No. 11304371, and No. 2014CB921500). J.S.Z. and J.B.G. are supported by NSF MIRT (DMR 1122603, DMR 0904282) and the Robert A Welch foundation (Grant No. F-1066).

*Corresponding author: jgcheng@iphy.ac.cn

¹B. J. Kim, H. Jin, S. J. Moon, J.-Y. Kim, B.-G. Park, C. S. Leem, J. Yu, T. W. Noh, C. Kim, S.-J. Oh, J.-H. Park, V. Durairaj, G. Cao, and E. Rotenberg, *Phys. Rev. Lett.* **101**, 076402 (2008).

²B. J. Kim, H. Ohsumi, T. Komesu, F. Sakai, T. Morita, H. Takagi, and T. Arima, *Science* **323**, 1329 (2009).

³K. Ohgushi, H. Gotou, T. Yagi, Y. Kiuchi, F. Sakai, and Y. Ueda, *Phys. Rev. B* **74**, 241104(R) (2006).

⁴G. Cao, J. E. Crow, R. P. Guertin, P. F. Henning, C. C. Homes, M. Strongin, D. N. Basov, and E. Lochner, *Solid State Commun.* **113**, 657 (2000).

⁵S. J. Moon, H. Jin, K. W. Kim, W. S. Choi, Y. S. Lee, J. Yu, G. Cao, A. Sumi, H. Funakubo, C. Bernhard, and T. W. Noh, *Phys. Rev. Lett.* **101**, 226402 (2008).

⁶J. G. Zhao, L. X. Yang, Y. Yu, F. Y. Li, R. C. Yu, Z. Fang, L. C. Chen, and C. Q. Jin, *J. Appl. Phys.* **103**, 103706 (2008).

⁷J.-M. Carter, V. V. Shankar, M. A. Zeb, and H.-Y. Kee, *Phys. Rev. B* **85**, 115105 (2012).

⁸M. A. Zeb and H.-Y. Kee, *Phys. Rev. B* **86**, 085149 (2012).

⁹J. M. Longo, J. A. Kafalas, and R. J. Arnett, *J. Solid State Chem.* **3**, 174 (1971).

¹⁰G. Cao, V. Durairaj, S. Chikara, L. E. DeLong, S. Parkin, and P. Schlottmann, *Phys. Rev. B* **76**, 100402(R) (2007).

¹¹J. G. Cheng, J. A. Alonso, E. Suard, J. S. Zhou, and J. B. Goodenough, *J. Am. Chem. Soc.* **131**, 7461 (2009).

¹²J.-G. Cheng, J.-S. Zhou, J. A. Alonso, J. B. Goodenough, Y. Sui, K. Matsubayashi, and Y. Uwatoko, *Phys. Rev. B* **80**, 104430 (2009).

¹³H. Kojitani, A. Furukawa, and M. Akaogi, *Am. Mineral.* **92**, 229 (2007).

¹⁴F. Izumi and K. Momma, *Solid State Phenom.* **130**, 15 (2007).

¹⁵H. Toraya, *J. Appl. Cryst.* **23**, 485 (1990).

¹⁶V. Sidey, *J. Appl. Cryst.* **37**, 1013 (2004).

¹⁷G. Cao, J. Bolivar, S. McCall, J. E. Crow, and R. P. Guertin, *Phys. Rev. B* **57**, R11039 (1998).

¹⁸J.-G. Cheng, J.-S. Zhou, J. B. Goodenough, Y. Sui, Y. Ren, and M. R. Suchomel, *Phys. Rev. B* **83**, 064401 (2011).

¹⁹K. Ohgushi, T. Yagi, H. Gotou, Y. Kiuchi, and Y. Ueda, *Physica B* **404**, 3261 (2009).

²⁰J. G. Zhao, L. X. Yang, Y. Yu, F. Y. Li, R. C. Yu, and C. Q. Jin, *Inorg. Chem.* **48**, 4290 (2009).

²¹J. B. Goodenough, J. A. Kafalas, and J. M. Longo, *High-Pressure Synthesis. Preparative Methods in Solid State Chemistry* (Academic Press, Inc., New York and London, 1972).

²²C.-Q. Jin, J.-S. Zhou, J. B. Goodenough, Q. Q. Liu, J. G. Zhao, L. X. Yang, Y. Yu, T. Katsura, A. Shatskiy, and E. Ito, *Proc. Natl. Acad. Sci.* **105**, 7115 (2008).

²³W. A. Harrison, *The Electronic Structure and Properties of Solids* (Freeman, San Francisco, 1980).

²⁴K. Ohgushi, J.-i. Yamaura, H. Ohsumi, K. Sugimoto, S. Takeshita, A. Tokuda, H. Takagi, M. Takata, and T.-h. Arima, *Phys. Rev. Lett.* **110**, 217212 (2013).